

Predicting The One-Particle Density Matrix With Machine Learning

S. Hazra,¹ U. Patil,¹ and S. Sanvito¹

¹*School of Physics and CRANN Institute, Trinity College, Dublin 2, Ireland*

(Dated: January 15, 2024)

Two of the most widely used electronic structure theory methods, namely Hartree-Fock and Kohn-Sham density functional theory, both require the iterative solution of a set of Schrödinger-like equations. The speed of convergence of such self-consistent field process depends on the complexity of the system under investigation and on the initial guess for the density matrix. An initial density matrix close to the ground-state one will effectively allow one to cut out many of the self-consistent steps necessary to achieve convergence. Here, we predict the density matrix of Kohn-Sham density functional theory by constructing a neural network, which uses the atomic positions as only information. Such neural network provides an initial guess for the density matrix far superior to any other recipes available, in particular for molecules with metallic bonds. Furthermore, the quality of such neural-network density matrix is good enough for the evaluation of interatomic forces. This allows us to run accelerated *ab-initio* molecular dynamics with little to no self-consistent steps.

I. INTRODUCTION

Density functional theory (DFT) [1–3] has been playing a central rôle in the electronic structure calculations of molecules and solids for more than six decades. The DFT success boils down to the rigorous theoretical framework [1], to the availability of well-controlled approximations of the exchange-correlation functional [4], to the multitude of numerical implementations [5–11], and to the community rigor in benchmarking results [12]. In principle, for a given functional one can find the ground-state density and energy by functional minimization, a procedure denoted as orbital-free DFT [13–15]. However, the lack of a universal and accurate approximation to a functional form of the non-interacting kinetic energy, a shortfall hardly mitigated by machine learning (ML) [16], makes the widespread use of orbital-free DFT impractical. The problem can be circumvented by the Kohn-Sham (KS) construct [2], in which the minimization of the functional is performed by solving an associated system of single-particle Schrödinger-like equations. The one-particle potential entering the KS equations does, in turn, depend on the electron density. Hence, the solution is iterative and requires a multi-step cycle, where the electron density and the KS potential are continuously updated until convergence is reached. Such self-consistent field (SCF) process is common to other electronic structure methods, for instance the Hartree-Fock scheme, where one updates the coefficients of the molecular orbitals [17].

In general the number of iterations required by the SCF process to achieve the desired accuracy depends on the system’s complexity, the particular numerical implementation and the initial trial electron density. Systems presenting a band gap are typically easier to converge than metals, since oscillations in the electron density during the iterative convergence are largely suppressed. Such oscillations can be damped by selecting appropriate ways to update the charge density from an iteration to the next, a process that in general largely determines the rate at which convergence is achieved. Typically one

mixes the charge density output of previous iterations to determine the new input. The direct inversion of the iterative subspace (DIIS) method, proposed by Pulay [18, 19], is probably the most widely used SCF-solver in modern DFT codes. However, there exists a multitude of alternative schemes and refinements, whose performance depends on the specific problem at hand [20–28].

Regardless of the mixing method used, an initial guess for the charge density close to the final self-consistent solution will speed up convergence, by typically reducing the number of iterations to perform. Such an initial density is usually defined either over a real-space or a k -space grid, in DFT codes based on plane waves, or in the form of a one-particle density matrix (DM), for local-orbital codes. There are multiple strategies to generate the initial charge density (or the DM), which all reduce to solve an associated non-self-consistent problem of some kind. As several of such schemes will be explored here, a detailed description will be provided in our method section.

The main aim of our work is to construct ML models, namely neural networks, to learn the ground-state one-particle DM of a DFT calculation. The models are based on structural and atomic information only, namely the chemical nature and positions of the atoms forming a molecule. The so-constructed DM can then be used either as a starting point for a SCF cycle or, if the accuracy is good enough, to perform a non-self-consistent evaluation of the various observables, for instance energy and forces. Note that ML schemes to generate the charge density in either real space [29–32] or over an atom-center basis [33] have been already proposed. One can then, in principle, take one of such models and try to construct the DM from the computed charge density. This strategy, however, requires projection across different incomplete basis sets, a process that inevitably introduces additional errors. These are likely to be large enough to preclude the use of the ML DM, namely this will be unlikely competitive with other initial-density generation approaches. Furthermore, learning the DM directly enables the straightforward evaluation of the expectation values of all one-particle operators. These include non-

local potentials, so that the same scheme can be used with Hartree-Fock calculations. Note that a mapping between the external potential and the one-particle density matrix, constructed over a kernel ridge regression, been recently proposed [34].

The paper is organised as follows. In the next section we discuss the main methodological aspects of the models construction and the DFT implementation used to generate the data and benchmark the results. Then, we proceed by presenting the results. In particular, we first evaluate the quality of our DM as starting point for a SCF cycle, and then we analyse the error on the predicted energy and forces. With these results at hand we perform non-self-consistent *ab initio* molecular dynamics, whose results are compared with fully converged one. Finally, we conclude and suggest possible future directions.

II. METHODS

All the electronic structure theory calculations performed in this work to generate the training dataset and to benchmark the results have been produced with the open source Python package, PySCF [11, 35]. This numerically implements all-electron DFT and a number of quantum-chemistry methods, such as Hartree-Fock, over a Gaussian basis set. For all our calculations we have used the cc-pVDZ basis, formed by double-zeta polarised orbitals for the valence electrons. Thus, for the atomic species relevant for our tests we have 5 basis functions for H, 14 for O, 18 for S and 43 for Fe. In fact, three different molecule have been considered in this work, namely H_2O , S_2O and $[\text{Fe}(\text{H}_2\text{O})_6]^{2+}$, see Fig. 1.

We start our analysis with H_2O (C_{2v} symmetry), since this presents a simple electronic structure and typically no convergence problems. Its charge density, however, does not differ much from a superposition of atomic densities, so that a more stringent test is provided by S_2O (also C_{2v} symmetry). Importantly, both H_2O and S_2O can be described by only three structural features, so that the more complex $[\text{Fe}(\text{H}_2\text{O})_6]^{2+}$ (O_h symmetry) is investigated last. The $[\text{Fe}(\text{H}_2\text{O})_6]^{2+}$ molecule also gives us the opportunity to test our method for a metal bond. All electronic structure calculations are performed with the BLYP functional, which combines the generalised gradient approximation for the exchange energy of Becke [36] with the Lee-Yang-Parr correlation energy [37]. The SCF cycle is converged with the DIIS scheme [18, 19] for H_2O and S_2O , while for $[\text{Fe}(\text{H}_2\text{O})_6]^{2+}$ we employ a second-order solver (SOS) [27, 28], as the convergence appears more problematic.

Since our ML DM will be compared with that generated by conventional initial guesses, it is worth spending some time in describing these. Possibly, the simplest choice constructs the charge density as a superposition of atomic densities, while the DM is obtained from the orbitals that diagonalize the Fock matrix associated to such spin-restricted guess density. This is the ‘minao’ PySCF

default option. Alternatively, one can use the eigenstates of the non-interacting problem, namely those orbitals that diagonalize an Hamiltonian comprising only the kinetic energy and the nuclear potential. This is the one-electron DM, ‘1e’ option in PySCF, which usually represents a poor starting point for molecules [38]. Then, there are options based on spin-restricted atomic Hartree-Fock calculations (‘atom’ and ‘huckel’ in PySCF), employing different recipes for the construction of the guess orbitals used to compute the DM [38, 39]. Finally, one can use the orbitals resulting from a pre-tabulated initial potential [39], ‘vsap’ option.

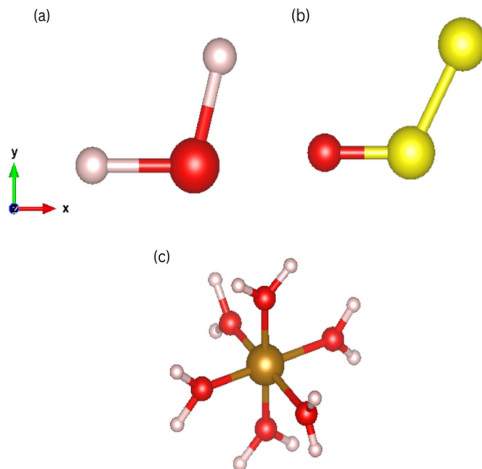


Figure 1: The molecules investigated in this study placed in their default positions along the Cartesian axes: (a) H_2O , (b) S_2O , and (c) $[\text{Fe}(\text{H}_2\text{O})_6]^{2+}$. Color code: H = white, O = red, Fe = dark golden, S = yellow, x -axis = red, y -axis = green, z -axis = blue.

The main goal of this work is to replace the methods for constructing the initial guess DM described above with one obtained with ML. For this task, we use dense neural networks, where the input features are the independent Cartesian coordinates of the molecules and the outputs are the DM matrix elements. A summary of the structure of the different neural networks, together with the training-set errors, are reported in Table I. The use of the Cartesian coordinates together with a dense neural network effectively forces an equivariant quantity, namely the DM, to be described by an invariant model. This issue is here resolved by manually removing the rotational and translational degrees of freedom of the molecule, a procedure that makes the entire problem invariant. Of course, such solution is not general and a more elegant way to tackle the problem would be to use a fully equivariant representation of the molecular structure [40]. This, however, adds a significant new layer of complexity, which we wish to avoid for our early study. Thus, we remove the translational degrees of freedom by fixing a given atom at the origin. In particular, we use oxygen, the central sulphur and the Fe^{2+} cation,

Table I: Table summarising the structure and performance of the final neural networks trained for the three molecules. Here we report the number of features defining the input, N_{in} , the dimension of the DM, D_{DM} , the number of the network hidden layers, N_{hi} , the total number of neurons forming each hidden layer, N_{nu} , and the total number of weights, N_{w} . Then, we report the mean absolute error (MAE), the largest error on the matrix elements, $\delta\rho_{\text{max}}$, the root-mean square error (RMSE), and the R^2 coefficient of the DMs. All errors refer to the test sets and they are in atomic units (a.u.).

Molecule	N_{in}	D_{DM}	N_{hi}	N_{nu}	(N_{w})	MAE	$\delta\rho_{\text{max}}$	RMSE	R^2
H ₂ O	3	24×24	2	18, 32	662	0.0002	0.0057	0.0003	0.9999
S ₂ O	3	50×50	2	18, 28	583	0.0002	0.0112	0.0003	0.9999
[Fe(H ₂ O) ₆] ²⁺	6	187×187	2	16, 32	640	0.0002	0.0283	0.0005	0.9993

respectively for H₂O, S₂O and [Fe(H₂O)₆]²⁺. Then the rotational degrees of freedom are imposed by selecting an appropriate rotation. For the triatomic molecules, H₂O and S₂O, we constrain one atom on the negative x -axis and the second one in the x - y plane, so that the molecules are described by only three coordinates. In contrast, for [Fe(H₂O)₆]²⁺ we force the O atoms of the H₂O ligands to be on the three Cartesian axes and we consider only variation in the Fe-O bond length (the water molecules are taken as rigid). This returns us six independent coordinates (see Fig. 1).

The structure of the neural network has been optimized by varying the number of hidden layers and their size, by minimizing the mean absolute error (MAE). The optimal configuration for each molecule is reported in Table I. Note that in all cases we employ the exponential linear unit activation function. The datasets used to construct the model are form by 9,000 configurations for the training set, 800 for validation and 1,000 for testing. In the case of H₂O and S₂O such configurations are extracted from *ab-initio* Born-Oppenheimer molecular dynamics trajectories at 150 K, also performed with PySCF. In particular, we run for 117 and 130 picoseconds, respectively for H₂O and S₂O, by using the Nose-Hoover thermostat through the pyLammps API as implemented in LAMMPS package [41]. In contrast, for the case of [Fe(H₂O)₆]²⁺ we consider random rigid displacement of the H₂O molecules, such that the Fe-O bond length is varied within 10% from its equilibrium value (2.0525 Å). These return us training-set mean absolute errors (MAEs) of the order of 10^{-3} atomic units (a.u.). Note that typically, the largest DM matrix elements are found along the diagonal and they can reach values close to unity, while a significant fraction of the off-diagonal matrix elements remain small. For example, for the H₂O molecule we find 8.15% of the matrix elements, ρ , having values $0.1 < |\rho| < 1$, 43.75% in the range $10^{-3} < |\rho| < 0.1$ and 48.1% being $|\rho| < 10^{-3}$. The parity plots associated to our neural networks, together with the typical matrix elements distributions can be found in the Appendix.

Finally, we perform tests on how the computed DM can drive molecular dynamics, namely we perform *ab-initio* molecular dynamics using our ML DM and not the one resulting from a SCF cycle. In this case spe-

cial care must be taken, since the neural networks return DM only for molecules having the specific spatial orientations described before. For this reason, we operate the following workflow. A molecule at an arbitrary position is translated back to the origin and rotated so to have the orientation required by the neural networks. Then, the DM is evaluated with the network and used as a starting guess for a static DFT calculation (non-self-consistent). Energy and forces are thus evaluated using PySCF. The molecule is then rotated/translated back to the original position and the same rotation is applied to the forces. Such force field is input into the molecular dynamics package, which updates the atomic coordinates. Then the process is repeated. The molecular dynamics steps are implemented in the LAMMPS package [41].

III. RESULTS AND DISCUSSIONS

In order to validate our entire approach we perform three different tests. Firstly, we evaluate the efficacy of the ML DM as a starting point for a SCF cycle. Then, we quantify the accuracy of the DM in determining energy and forces. Finally, we compare the molecular-dynamics trajectories driven by the forces associated to the ML DM with those of fully self-consistent *ab-initio* molecular dynamics.

A. Machine-learning DM as initial guess

The first test consists in evaluating how accurate is the DM generated by the neural networks as starting point for the DFT SCF cycle. The test is performed over 1000 new configurations for each molecule and in Fig. 2 we report the average number of SCF iterations performed to achieve convergence and their associated variance. In this case converge is defined by having an energy difference between subsequent iterations lower than 10^{-9} Ha, a value that sets a rather tight convergence criterion. For this test we perform two sets of calculations, where the SCF cycles are driven respectively by the DIIS or the SOS mixing scheme, with convergence parameters set by the PySCF default.

In general we find the SOS DM-update strategy to be significantly more performing than the simpler DIIS, with the total number of iterations reducing by approximately a factor three regardless of the molecule or the initial DM. Note that this advantage is partially compensated by the SOS scheme being numerically heavier than DIIS, namely a single iteration takes longer. We have also found that sometimes for $[\text{Fe}(\text{H}_2\text{O})_6]^{2+}$ and the DIIS solver, 50 iterations are not enough to achieve convergence. This is somehow expected considering the electronic structure of the $[\text{Fe}(\text{H}_2\text{O})_6]^{2+}$ cation. In fact, $[\text{Fe}(\text{H}_2\text{O})_6]^{2+}$ is a spin-crossover molecule presenting a temperature-induced low-spin to high-spin transition, driven by a distortion of the octahedral coordination shell of the Fe^{2+} ion. This is only partially described by DFT [42], and a multi-determinant theory appears more appropriate [43]. For this reason it is not surprising that for some highly distorted configurations our non-spin-polarised DFT calculations struggle to converge. Note that this is not so crucial here, since we are not seeking to compute the exact ground state of $[\text{Fe}(\text{H}_2\text{O})_6]^{2+}$, but simply to present a test example for ‘difficult’ convergence. In any case, when convergence is not achieved, the SCF cycle is stopped after 50 iterations.

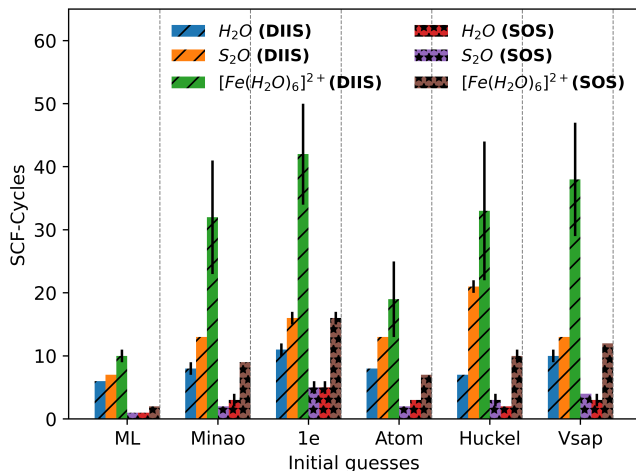


Figure 2: Total average number of SCF steps taken to achieve convergence for different starting DMs and mixing schemes. Here the convergence criterion is on the total energy between two consecutive SCF steps that should be lower than 10^{-9} Ha. The black bars around the mean indicate the variance. Variances lower than one iteration are not displayed.

Despite these differences, the convergence-speed trends with respect to the initial DM are rather similar across the two mixing schemes, so that in our discussion we refer first to data obtained with the SOS algorithm. As expected the H_2O and S_2O molecules converge significantly faster than $[\text{Fe}(\text{H}_2\text{O})_6]^{2+}$, as their simple covalent bonding structure would suggest. Also as expected, the simple ‘1e’ default provides the worst starting DM

and convergence is achieved in five iterations for H_2O and S_2O and about 16 for $[\text{Fe}(\text{H}_2\text{O})_6]^{2+}$. The other conventionally constructed starting DMs appear to perform rather similarly to each other with the two covalently bonded molecules converging in about 3-4 SCF steps, and $[\text{Fe}(\text{H}_2\text{O})_6]^{2+}$ in about 10. Most importantly, our DM significantly outperforms any other methods, with a single SCF iteration being necessary for H_2O and S_2O , while $[\text{Fe}(\text{H}_2\text{O})_6]^{2+}$ requires only two. This gives us a speedup in the computation of the SCF cycle comprised between a factor 3 and a factor 5. Note that the speedup is less pronounced when the DIIS mixing scheme is used, in particular for the covalently bonded molecules, where the advantage over the other schemes is only fractional. This difference seems to boil down to the inefficiency of the mixing scheme, which brings the iteration count to 6-7 even when the calculation is initiated with the ML DM.

B. Convergence analysis

We now look in more detail at how convergence is achieved for different starting DMs and the two different mixing schemes. We begin by considering H_2O and then move to $[\text{Fe}(\text{H}_2\text{O})_6]^{2+}$, with the results for S_2O being somehow in between these two cases. In figure 3, we show the total energy (with respect to the ground-state energy) as a function of the iteration number, n , for H_2O computed with the DIIS [panel (a)] and SOS [panel (b)] mixing scheme. Furthermore, in panel (c) we present the norm of the difference between the ground state (converged) DM, ρ^{GS} , and that at the n -th iteration, ρ^n , also along the DIIS-driven SCF cycle. This last quantity is computed as $\Delta\rho = \sum_{ij} |\rho_{ij}^{\text{GS}} - \rho_{ij}^n|$, with ρ_{ij} being the i, j DM matrix element. Although the detail of each SCF cycle may differ depending on the molecule geometry, the figure shows a typical case.

In general all initial DMs are somewhat different from the final ground-state one, with the largest variations found, as expected, for the ‘1e’ initialization (the total energy difference at $n = 0$ is in excess of 8 Ha and it is not displayed here). The convergence is then monotonic, when the SOS solver is used, while it may present oscillations for DIIS. This explains the largest number of iterations typically taken by DIIS. Stinkingly the ML-generated DM appears extremely close to the final ground-state one, so that the convergence is monotonic in all cases. In fact, the $n = 0$ computed total energies for H_2O are on average within 10^{-4} Ha from their ground-state value and the percentage variation of the DM at the first iteration is only 0.196%. This suggests that, by large, the ML-DM already provides an excellent estimation of the ground-state density matrix. As a comparison the second best initial DM appears to be that generated with a restricted Hartree-Fock calculation (‘huckel’ option), with an initial total energy error of about 10^{-2} Ha. All the others DM-generating schemes

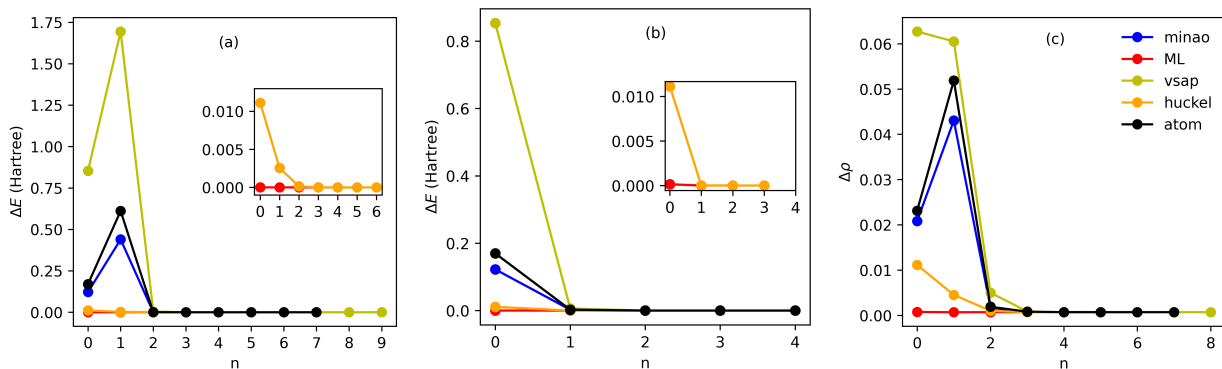


Figure 3: Analysis of the SCF cycle for H₂O. In panels (a) and (b) we show the total energy (measured with respect to the ground-state energy) as a function of the iteration number, n , for convergence driven by the DIIS and SOS mixing scheme, respectively. In panel (c) we present the norm of the difference between the ground-state converged DM, ρ^{GS} , and that computed at the n -th iteration, ρ^n . In this case we follow the DIIS-driven SCF cycle. The insets zoom in around the $n = 0$ regions, corresponding to the initial DM.

have an initial error larger than 0.1 Ha.

The path to convergence becomes significantly more oscillatory when one looks at the DIIS SCF cycle for $[\text{Fe}(\text{H}_2\text{O})_6]^{2+}$ (see Fig. 4). This time, the energy and DM fluctuations are significantly more pronounced, with the appearance of ‘spikes’ in correspondence to some self-consistent steps when using the DIIS solver. These originate from fluctuations in atomic orbital occupation across different SCF iterations. Such large fluctuations are suppressed by the SOS mixing scheme, which reinstates a monotonic approach to the ground-state solution. Most importantly, also for $[\text{Fe}(\text{H}_2\text{O})_6]^{2+}$ the ML-constructed DM provides a much more accurate starting point. In fact, it is sufficiently accurate that the oscillations are suppressed, regardless of the mixing scheme. Furthermore, already at the first iteration energy and DM are extremely accurate. This time, the average energy is about 3×10^{-5} Ha away from the converged one (this corresponds to an error $1.7 \times 10^{-6}\%$), while the percentage variation of the DM at the first iteration with respect to the ground state is 0.77%.

C. Non-self-consistent forces

The previous section has shown that the ML DM requires an extremely limited number of SCF iterations to achieve the desired convergence and that, even without any iteration, it can already provide an accurate estimate of the DFT total energy. Here we explore further this second aspect and investigate the accuracy of our ML DM in predicting a second observable, namely the atomic forces. For this section we consider the S₂O molecule in particular, but the results for H₂O and $[\text{Fe}(\text{H}_2\text{O})_6]^{2+}$ are qualitatively rather similar.

In figure 5 we present the parity plot diagram for the x [upper panel] and y [lower panel] component of the atomic forces acting on the atom lying in the x - y plane.

These are computed for a set of 1000 distorted molecules obtained from the molecular dynamics trajectory used to generate the training set, but never used in the construction of the neural network. Since, the molecule are, by construction, always aligned in the x - y plane, there are no forces along z . The parity plot compares the fully converged DFT forces (y axis) with those predicted from the ML DM without operating any SCF iteration (x axis). Points on the parity line are predicted exactly. The graphs also show histograms of the distributions of the atomic forces. Note that along our molecular-dynamics trajectory the forces can be as large as $2 \text{ eV}/\text{\AA}$, but typically they are concentrated within $\pm 0.25 \text{ eV}/\text{\AA}$.

Clearly, there is an extremely good mapping between the ML-DM-predicted forces and the exact ones, with the vast majority of the points staying on the parity line. This is reflected in the almost identical force distributions. Quite interestingly, there is no biased distribution of errors across the range of force magnitude explored, in contrast to what usually found for ML force fields, where the largest error is encountered for small forces. The mean absolute error (MAE) is calculated at $126 \text{ meV}/\text{\AA}$ and $62 \text{ meV}/\text{\AA}$, respectively for the x and y component. Such error can be further reduced by noticing that the ML-generated DM does not necessarily describe an integer number of electrons. This feature can be corrected by re-scaling the ML-generated DM of a factor N_e/N_e^{ML} , where N_e is the total number of electrons and N_e^{ML} that computed using the as-generated ML DM, $N_e^{\text{ML}} = \text{Tr}[\rho^{\text{ML}} \cdot S]$, with S being the overlap matrix. For S₂O we find that typically N_e^{ML} is less than 0.1% different from N_e , but the correction is enough to bring down the MAE to $62 \text{ meV}/\text{\AA}$ and $22 \text{ meV}/\text{\AA}$, respectively for the x and y component (the parity plots of Fig. 5 have been obtained with the forces computed after such DM re-scaling). This error is significantly lower than what typically found for state-of-the-art force fields [44–46]. Although a thorough comparison is not

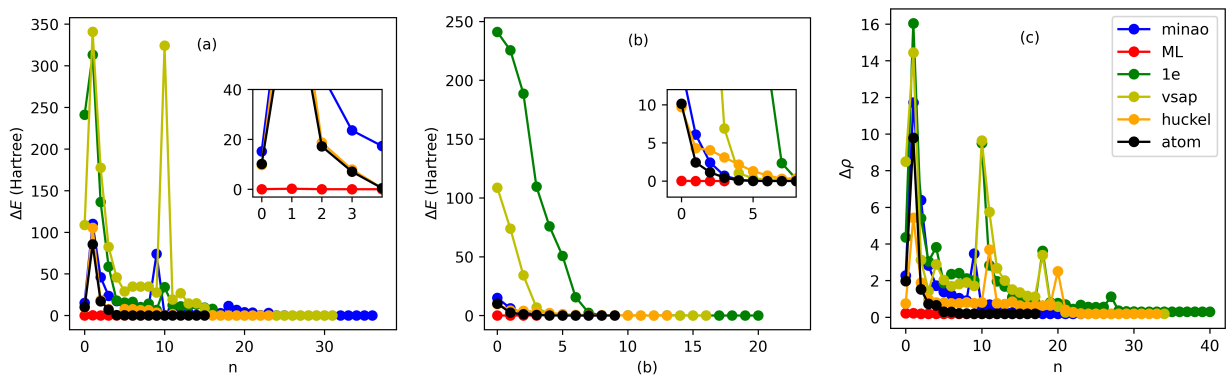


Figure 4: Analysis of the SCF cycle for $[\text{Fe}(\text{H}_2\text{O})_6]^{2+}$. In panels (a) and (b) we show the total energy (measured with respect to the ground-state energy) as a function of the iteration number, n , for convergence driven by the DIIS and SOS mixing scheme, respectively. In panel (c) we present the norm of the difference between the ground-state converged DM, ρ^{GS} , and that computed at the n -th iteration, ρ^n . In this case, we follow the SH: DIIS-driven SCF cycle. The insets zoom in around the $n = 0$ regions, corresponding to the initial DM.

simple, since the analysis needs to be carried out with the same molecules, same training set size, etc., this result clearly demonstrates that predicting the DM to be used in non-self-consistent DFT, can be a valid alternative to the construction of a force field. Namely, the forces obtained from the ML-predicted DM can be used as driver for molecular dynamics. This aspect is explored last in the next section.

D. Non-self-consistent molecular dynamics

As a final test, we now perform molecular dynamics simulations by using the ML-predicted DM. In particular, we use the forces obtained after rescaling the DM by N_e/N_e^{ML} and after a single SCF step. Such step is needed, since the re-scaled DM seems to have a total energy marginally lower than that of the ground state. The molecular dynamics simulations are then performed at 150K for S_2O and H_2O for total of 0.14 and 0.12 nanoseconds, respectively. In both cases we use the rotation procedure described in the method section to avoid the need of an equivariant model. The trajectories obtained are then compared with the fully converged *ab-initio* ones, and with those computed by performing only a single DIIS self-consistent step, starting from the PySCF default ‘minao’ charge density.

The different molecular dynamics trajectories are monitored and compared by looking at the bond length and bond angle thermal distributions, which are presented in Fig. 6 for the two molecules. In the case of H_2O [panels (c) and (d)] there is no significant difference between the various methods, with rather similar distributions. This has to be expected considering the speed of convergence of the SCF cycle in this case. Thus, we find an average O-H bond length of about 0.9837 Å and an average bond angle of 101.83°, values fully consistent with the static

DFT BLYP results, 0.9751 Å and 104.14°, and with the experimental values of 0.9578 Å and 104.47° [47].

The S_2O case is, instead, quite different. From panels (a) and (b) of Fig. 6 one can appreciate that the ML DM provides an excellent estimate of the fully DFT-converged one, so that the thermal distributions of bond lengths and angle are rather similar to those obtained with fully *ab-initio* molecular dynamics. In this case there are three bond lengths corresponding to the S-O bond, the S-S one and the second S-O distance between the two most peripheral atoms. The centers of the distributions are close to the reported experimental values of 1.4650 Å (S-O), 1.8834 Å (S-S) and 3.2505 Å (S-S) [47], and so is the bond angle, 117.876°, with the remaining differences being attributed to the choice of exchange and correlation energy. This is not the case when the molecular dynamics is performed with a single SCF step starting from the PySCF ‘minao’ initialization. In fact, the low accuracy in the determination of the forces results in an average structure presenting a significantly compressed S-S bond and a drastic reduction in the bond angle.

Finally, in Fig. 7 we present the decomposition of the total energy over the one-electron, H_{one} , Coulomb (Hartree), H_{C} , exchange-correlation, H_{XC} , and nucleus-nucleus, H_{NN} , components. As expected, since the average structures are erroneously predicted, the minao-initialized molecular dynamics provides distributions pretty far from those obtained with self-consistent DFT. This contrasts the results obtained from our ML DM, which not only describes well the structure, but also all energy components.

IV. CONCLUSION

We have shown that neural networks can be trained to predict the one-particle density matrix required by

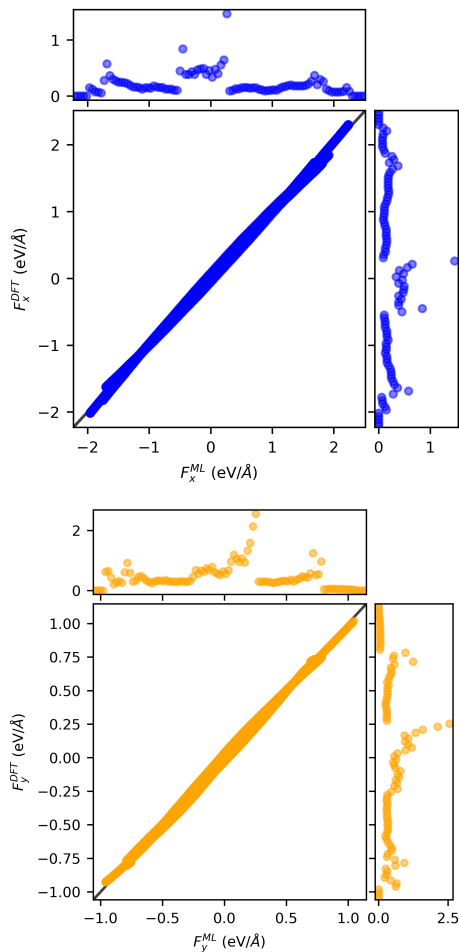


Figure 5: Parity plot for the $\alpha = x, y$ component of the atomic forces computed by using the ML DM, F_{α}^{ML} , with one SCF cycle, against the fully converged DFT ones, F_{α}^{DFT} . Data are here presented for a set of 1000 S_2O molecules extracted from the same molecular dynamics trajectory used to generate the training set. The upper panel is for the forces x component, while the lower panel is for the y component. The histograms on the side describes the frequency of the forces in the test set.

electronic-structure theories constructed over atomic-orbital basis sets. These ML DMs are of sufficient quality to be used as initial guess in Kohn-Sham DFT, demonstrating a reduction in the number of the self-consistent steps needed to achieve convergence over all other common initial choices. Equally important, such DMs return rather accurate energy and forces even without self-consistency, a fact that enables one to run inexpensive molecular dynamics simulations, whose computational cost is similar to that needed by machine-learning force fields. We have shown here results for three molecules, H_2O , S_2O and $[\text{Fe}(\text{H}_2\text{O})_6]^{2+}$, and density functional theory, but the method is agnostic to the system to de-

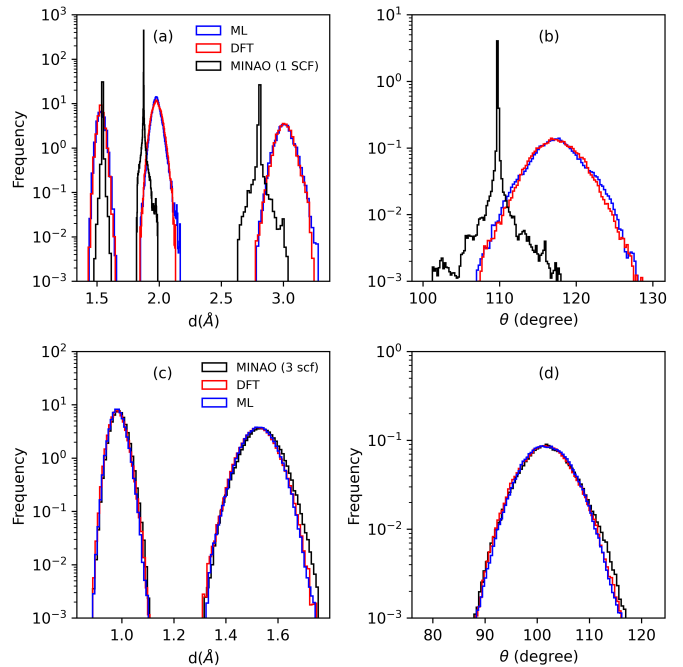


Figure 6: Histograms of the bond lengths, d , and bond angles, θ , along the molecular dynamics trajectories for S_2O [panels (a) and (b)] and H_2O [panels (c) and (d)]. There are two distinct bond lengths for H_2O , namely O-H and H-H, while there are three for S_2O , namely two S-O and one S-S.

scribe and the choice of electronic structure theory, as long as this is based on the density matrix. For instance, it can be employed together with wave-function-based quantum-chemistry methods such as Hartree-Fock. It is also important to note that, although here the molecule structure is represented by simple Cartesian coordinates, our proposed method can be implemented with more sophisticated structural descriptors. These can be constructed equivariant [53] and can be descriptive enough to avoid the need of using deep-learning machine-learning models [46].

The drawback of our scheme is that the number of matrix elements to predict scales quadratically with the number of basis functions used in the calculation, so that it becomes increasingly expensive as the system size grows. In practice, many of the matrix elements remain rather small and they can be safely neglected when evaluating the DM for accurate non-self-consistent electronic structure or molecular dynamics. In any case, our scheme remains convenient as long as the overarching electronic structure method scales severely with the system size. In this case, the quadratic scaling of the DM construction is overshadowed by the computational cost to run long self-consistent cycles, and significant savings in computational overheads can be achieved. This can be the case, for instance, of post-Hartree-Fock schemes.

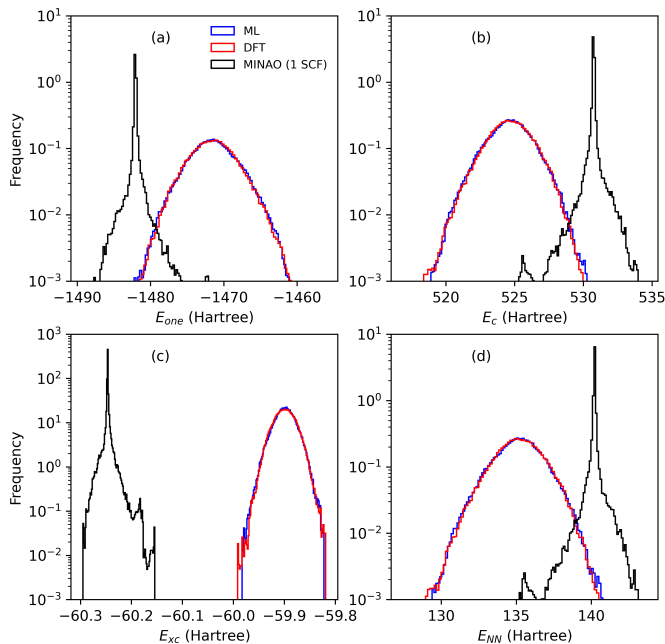


Figure 7: Histogram of the various energy components along the different molecular dynamics trajectories for the S_2O molecule. Here we separate the total energy into one-electron, H_{one} , Coulomb (Hartree), H_C , exchange-correlation, H_{XC} , and nucleus-nucleus, H_{NN} , components.

ACKNOWLEDGMENTS

This work has been supported by the Government of India, NOS Award (K-11015/65/2020-SCD-V/NOS), and by the Irish Research Council postgraduate program (MC). UP thanks the Qatar National Research Fund

(NPRP12S-0209-190063) for financial support. We acknowledge the DJEI/DES/SFI/HEA Irish Trinity Centre for High Performance Computing (TCHPC) for the provision of computational resources.

V. APPENDIX

A. Neural-network parity plots

In Fig. 8 we present the parity plots (in logarithmic scale) for the elements of the density matrix of H_2O [panels (a) and (d)], S_2O [panels (b) and (e)] and $[\text{Fe}(\text{H}_2\text{O})_6]^{2+}$ [panels (c) and (f)]. The upper panels are for the training set and the lower ones for the test set, and the value of the MAE is reported in all cases. As we can see there is an excellent agreement between the ML-computed DM and the fully converged DFT one, with most of the points lying on the parity line. This is true for matrix elements larger than $\sim 10^{-2}$, namely for those that have a dominant behaviour on all the observable of relevance (e.g. total energy and forces). Larger relative errors are found for smaller elements, for which the DFT data are already noisy and the ML model can hardly train. This distribution of errors reflects the rather low MAE reported for all cases (see also Table I). The only exception is for a few points in the training set of $[\text{Fe}(\text{H}_2\text{O})_6]^{2+}$, for which some more pronounced deviations are reported. These, however, correspond to situations where the DFT calculations struggle to converge (see main text) and the DM is the one obtained at the maximum number of self-consistent iterations allowed (hence, not the converged one). These training points are thus discarded. The test set, instead, contains only examples where full convergence is obtained.

-
- [1] P. Hohenberg and W. Kohn, *Inhomogeneous electron gas*, Phys. Rev. **136**, B864-B871 (1964).
 - [2] W. Kohn and L.J. Sham, *Self-consistent equations including exchange and correlation effects*, Phys. Rev. **140**, A1133-1138 (1965).
 - [3] R.G. Parr and W. Yang, *Density-Functional Theory of Atoms and Molecules*, Oxford University Press, New York (1994).
 - [4] J.P. Perdew and K. Schmidt, *Jacob's ladder of density functional approximations for the exchange-correlation energy*, AIP Conf. Proc. **577**, 1-20 (2001).
 - [5] G. Kresse and J. Hafner, *Ab initio molecular dynamics for liquid metals*, Phys. Rev. B **47**, R558-R561 (1993).
 - [6] P. Giannozzi, O. Andreussi, T. Brumme, O. Bunau, M. Buongiorno Nardelli, M. Calandra, R. Car, C. Cavazzoni, D. Ceresoli, M. Cococcioni, N. Colonna, I. Carnimeo, A. Dal Corso, S. de Gironcoli, P. Delugas, R. A. DiStasio Jr, A. Ferretti, A. Floris, G. Fratesi, G. Fugallo, R. Gebauer, U. Gerstmann, F. Giustino, T. Gorni, J. Jia, M. Kawamura, H.-Y. Ko, A. Kokalj, E. Küçükbenli, M. Lazzeri, M. Marsili, N. Marzari, F. Mauri, N. L. Nguyen, H.-V. Nguyen, A. Otero-de-la-Roza, L. Paulatto, S. Poncé, D. Rocca, R. Sabatini, B. Santra, M. Schlipf, A. P. Seitsonen, A. Smogunov, I. Timrov, T. Thonhauser, P. Umari, N. Vast, X. Wu, S. Baroni, *Advanced capabilities for materials modelling with Quantum ESPRESSO*, J. Phys.: Condens. Matter **29**, 465901 (2017).
 - [7] P. Blaha, K. Schwarz, F. Tran, R. Laskowski, G.K.H. Madsen and L.D. Marks, *WIEN2k: An APW+lo program for calculating the properties of solids*, J. Chem. Phys. **152**, 074101 (2020).
 - [8] A.H. Romero, D.C. Allan, B. Amadon, G. Antonius, T. Applencourt, L. Baguet, J. Bieder, F. Bottin, J. Bouchet, E. Bousquet, F. Bruneval, G. Brunin, D. Caliste, M. Côté, J. Denier, C. Dreyer, P. Ghosez, M. Giantomassi, Y. Gillet, O. Gingras, D.R. Hamann, G. Hautier, F. Jollet, G. Jomard, A. Martin, H.P.C. Miranda, F. Naccarato, G. Petretto, N.A. Pike, V. Planes, S. Prokhorenko, T. Rangel, F. Ricci, G.-M. Rignanese, M. Royo, M. Stengel, M. Torrent, M.J. van Setten, B.

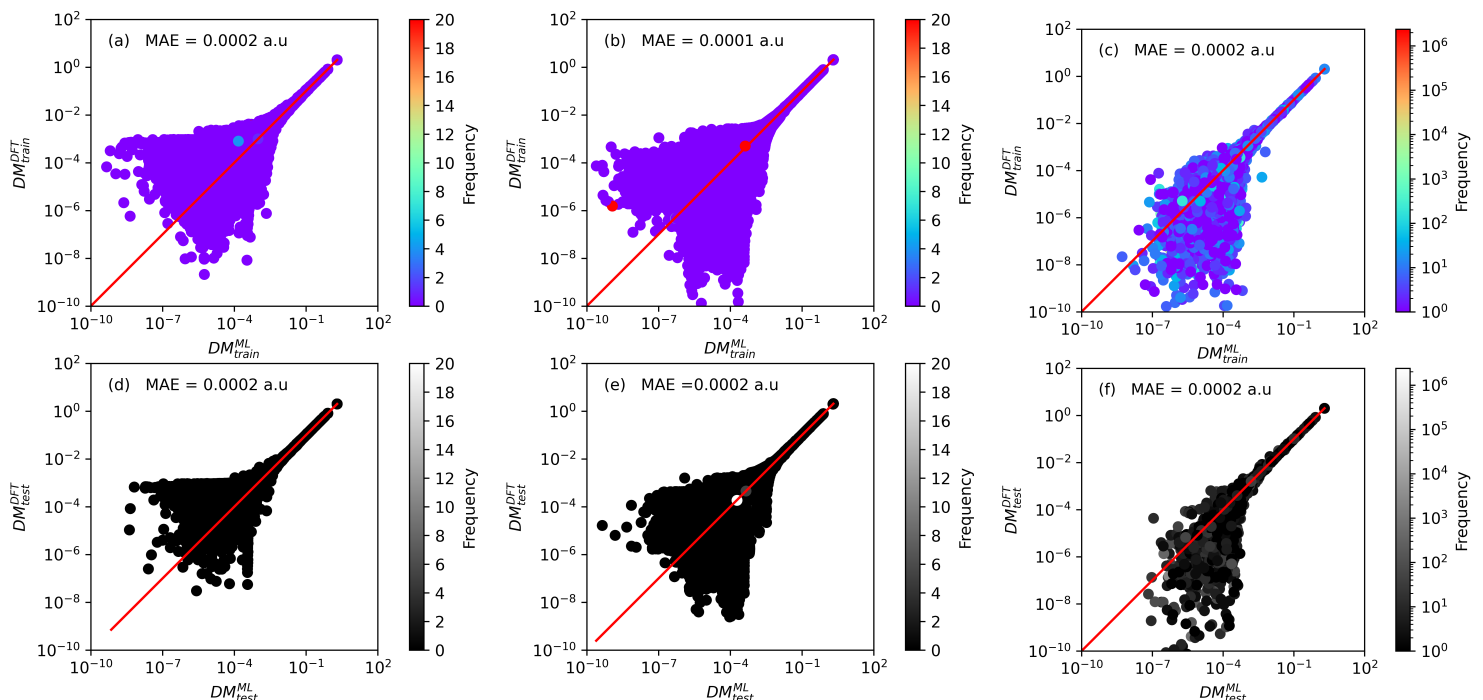


Figure 8: Parity plots for H_2O [panels (a) and (d)], S_2O [panels (b) and (e)], and $[\text{Fe}(\text{H}_2\text{O})_6]^{2+}$ [panels (c) and (f)]. The upper panels are for the training set, and the lower ones for the test one. Each graph reports also the MAE achieved. Note that all the parity plots are in logarithmic scale (we plot $|\rho_{ij}|$) and that deviations are only found for the smaller matrix elements. The colour code describes the density of given DM matrix-element values.

- Van Troeye, M.J. Verstraete, J. Wiktor, J.W. Zwanziger, X. Gonze, *ABINIT: Overview and focus on selected capabilities*, J. Chem. Phys. **152**, 124102 (2020).
- [9] V. Blum, R. Gehrke, F. Hanke, P. Havu, V. Havu, X. Ren, K. Reuter and M. Scheffler, *Ab initio molecular simulations with numeric atom-centered orbitals*, Comput. Phys. Commun. **180**, 2175-2196 (2009).
- [10] A. García, N. Papior, A. Akhtar, E. Artacho, V. Blum, E. Bosoni, P. Brandimarte, M. Brandbyge, J.I. Cerdá, F. Corsetti, R. Cuadrado, V. Dikan, J. Ferrer, J. Gale, P. García-Fernández, V.M. García-Suárez, Sandra García, G. Huhs, S. Illera, R. Korytár, P. Koval, I. Lebedeva, L. Lin, P. López-Tarifa, S.G. Mayo, S. Mohr, P. Ordejón, A. Postnikov, Y. Pouillon, M. Pruneda, R. Robles, D. Sánchez-Portal, J.M. Soler, R. Ullah, V. Wen-zhe Yu and J. Junquera, *SIESTA: Recent developments and applications*, J. Chem. Phys. **152**, 204108 (2020).
- [11] Q. Sun, X. Zhang, S. Banerjee, P. Bao, M. Barbry, N.S. Blunt, N.A. Bogdanov, G.H. Booth, J. Chen, Z.-H. Cui, J.J. Eriksen, Y. Gao, S. Guo, J. Hermann, M.R. Hermes, K. Koh, P. Koval, S. Lehtola, Z. Li, J. Liu, N. Mardirossian, J.D. McClain, M. Motta, B. Muscard, H.Q. Pham, A. Pulkin, W. Purwanto, P.J. Robinson, E. Ronca, E.R. Sayfutyarova, M. Scheurer, H.F. Schurkus, J.E.T. Smith, C. Sun, S.-N. Sun, S. Upadhyay, L.K. Wagner, X. Wang, A. White, J.D. Whitfield, M.J. Williamson, S. Wouters, J. Yang, J.M. Yu, T. Zhu, T.C. Berkelbach, S. Sharma, A.Yu. Sokolov, G. Kin-Lic Chan, *Recent developments in the PySCF program package*, J. Chem. Phys. **152**, 024109 (2020).
- [12] K. Lejaeghere, G. Bihlmayer, T. Björkman, P. Blaha, S. Blügel, V. Blum, D. Caliste, I.E. Castelli, S.J. Clark, A. Dal Corso, S. de Gironcoli, T. Deutsch, J.K. Dewhurst, I. Di Marco, C. Draxl, M. Dułak, O. Eriksson, J.A. Flores-Livas, K.F. Garrity, L. Genovese, P. Giannozzi, M. Giantomassi, S. Goedecker, X. Gonze, O. Grånäs, E.K.U. Gross, A. Gulans, F. Gygi, D.R. Hamann, P.J. Hasnip, N.A.W. Holzwarth, D. Iușan, D.B. Jochym, F. Jollet, D. Jones, G. Kresse, K. Koepnik, E. Küçükbenli, Y.O. Kvashnin, I.L.M. Locht, S. Lubeck, M. Marsman, N. Marzari, U. Nitzsche, L. Nordström, T. Ozaki, L. Paulatto, C.J. Pickard, W. Poelmans, M.I.J. Probert, K. Refson, M. Richter, G.-M. Rignanese, S. Saha, M. Scheffler, M. Schlipf, K. Schwarz, S. Sharma, F. Tavazza, P. Thunström, A. Tkatchenko, M. Torrent, D. Vanderbilt, M.J. van Setten, V. Van Speybroeck, J.M. Wills, J.R. Yates, G.-X. Zhang and S. Cottenier, *Reproducibility in density functional theory calculations of solids*, Science **351**, aad3000 (2016).
- [13] Y.A. Wang and E.A. Carter, *Orbital-Free Kinetic-Energy Density Functional Theory*, in S.D. Schwartz (ed.), *Theoretical Methods in Condensed Phase Chemistry. Progress in Theoretical Chemistry and Physics*, vol 5. Springer, Dordrecht (2002).
- [14] H. Chen and A. Zhou, *Orbital-free density functional theory for molecular structure calculations*, Numer. Math. Theor. Meth. Appl. **1**, 1-28 (2008).
- [15] T.A. Wesolowski and Y.A. Wang, *Recent Progress in Orbital-Free Density Functional Theory*, World Scientific (Singapore) (2013).

- [16] L. Li, J.C. Snyder, I.M. Pelaschier, J. Huang, U.-N. Niranjan, P. Duncan, M. Rupp, K.-R. Müller and K. Burke, *Understanding Machine-Learned Density Functionals*, Int. J. Quantum Chem. **116**, 819-83 (2016).
- [17] A. Szabo and N.S. Ostlund, *Modern Quantum Chemistry: Introduction to Advanced Electronic Structure Theory*, Dover Publications, New York (1996).
- [18] P. Pulay, *Convergence acceleration of iterative sequences - the case of SCF iteration*, Chem. Phys. Lett. **73**, 393-398 (1980).
- [19] P. Pulay, *Improved SCF convergence acceleration*, J. Comp. Chem. **3**, 556-560 (1982).
- [20] K.N. Kudin, G.E. Scuseria and E. Cancès, *A black-box self-consistent field convergence algorithm: One step closer*, J. Chem. Phys. **116**, 8255-8261 (2002).
- [21] K.N. Kudin and G. E. Scuseria, *Converging self-consistent field equations in quantum chemistry - recent achievements and remaining challenges*, ESAIM: M2AN **41**, 281-296 (2007).
- [22] E. Cancès and C. L. Bris, *Can we outperform the DIIS approach for electronic structure calculations?*, Int. J. Quantum Chem. **79**, 82-90 (2000).
- [23] V.R. Saunders and I.H. Hillier, *Level-shifting method for converging closed shell Hartree-Fock wave-functions*, Int. J. Quant. Chem. **7**, 699-705 (1973).
- [24] G.B. Bacskay, *A quadratically convergent Hartree-Fock (QC-SCF) method - application to closed shell systems*, Chem. Phys. **61**, 385-404 (1981).
- [25] S.P. Bhattacharyya, *Accelerated convergence in SCF calculations and level shifting technique*, Chem. Phys. Lett. **56**, 395-398 (1978).
- [26] X. Hu and W. Yang, *Accelerating self-consistent field convergence with the augmented Roothaan-Hall energy function*, J. Chem. Phys. **132**, 054109 (2010).
- [27] Q. Sun, *Co-iterative augmented Hessian method for orbital optimization*, arXiv preprint arXiv:1610.08423 (2016).
- [28] Q. Sun, J. Yang and G. Kin-Lic Chan, *A general second order complete active space self-consistent-field solver for large-scale systems*, Chem. Phys. Lett. **683**, 291 (2017).
- [29] F. Brockherde, L. Vogt, L. Li, M.E. Tuckerman, K. Burke and K.-R. Müller, *Bypassing the Kohn-Sham equations with machine learning*, Nat Commun. **8**, 872 (2017).
- [30] A. Chandrasekaran, D. Kamal, R. Batra, C. Kim, L. Chen and R. Ramprasad, *Solving the electronic structure problem with machine learning*, npj Comput. Mater. **5**, 22 (2019).
- [31] J.A. Ellis, L. Fiedler, G.A. Popoola, N.A. Modine, J.A. Stephens, A.P. Thompson, A. Cangi and S. Rajamanickam, *Accelerating finite-temperature Kohn-Sham density functional theory with deep neural networks*, Phys. Rev. B **104**, 035120 (2021).
- [32] B. Focassio, M. Domina, U. Patil, A. Fazzio and S. Sanvito, *Linear Jacobi-Legendre expansion of the charge density for machine learning-accelerated electronic structure calculations*, npj Comp. Mater. **9**, 87 (2023).
- [33] A. Grisafi, A. Fabrizio, B. Meyer, D.M. Wilkins, C. Corminboeuf and M. Ceriotti, *Transferable Machine-Learning Model of the Electron Density*, ACS Cent. Sci. **5**, 57-64 (2019).
- [34] X. Shao, L. Paetow, M.E. Tuckerman and M. Pavanello, *Machine Learning Electronic Structure Methods Based On The One-Electron Reduced Density Matrix*, Nature Commun. **14**, 6281 (2023).
- [35] Q. Sun, T.C. Berkelbach, N.S. Blunt, G.H. Booth, S. Guo, Z. Li, J. Liu, J.D. McClain, E.R. Sayfutyarova, S. Sharma, S. Wouters and G. Kin-Lic Chan, *PySCF: the Python-based simulations of chemistry framework*, WIREs Comput. Mol. Sci. **8**, e1340 (2018).
- [36] A.D. Becke, *Density-functional exchange-energy approximation with correct asymptotic behavior*, Phys. Rev. A **38**, 3098-3100 (1988).
- [37] C. Lee, W. Yang and R.G. Parr, *Development of the Colle-Salvetti correlation-energy formula into a functional of the electron density*, Phys. Rev. B **37**, 785-789 (1988).
- [38] S.Lehtola, *Assessment of initial guesses for self-consistent field calculations, Superposition of atomic potentials: simple yet efficient*, J. Chem. Theo. Comput. **15**, 1593-1604 (2019).
- [39] S.Lehtola, *Fully numerical calculations on atoms with fractional occupations and range-separated exchange functionals*, Phys. Rev. A **101**, 012516 (2020).
- [40] N. Thomas, T. Smidt, S. Kearnes, L. Yang, L. Li, K. Kohlhoff and P. Riley, *Tensor field networks: Rotation- and translation-equivariant neural networks for 3D point clouds*, arXiv:1802.08219 (2018).
- [41] J.S. Plimpton, *Fast Parallel Algorithms for Short-Range Molecular Dynamics*, Comp. Phys. **117**, 1-19 (1995); LAMMPS website: <https://www.lammps.org>, LAMMPS GitHub repository: <https://github.com/lammps/lammps>
- [42] A. Droghetti, D. Alfè and S. Sanvito, *Assessment of density functional theory for iron(II) molecules across the spin-crossover transition*, J. Chem. Phys. **137**, 124303 (2012).
- [43] A. Domingo, M.A. Carvajal and C. de Graaf, *Spin crossover in Fe(II) complexes: An ab initio study of ligand σ -donation* Int. J. Quantum Chem. **110**, 331 (2010).
- [44] R. Drautz, *Atomic cluster expansion for accurate and transferable interatomic potentials*, Phys. Rev. B **99**, 014104 (2019).
- [45] A.V. Shapeev, *Moment tensor potentials: A class of systematically improvable interatomic potentials*, Multiscale Modeling & Simulation **14**, 1153 (2016).
- [46] M. Domina, U. Patil, M. Cobelli and S. Sanvito, *Cluster expansion constructed over Jacobi-Legendre polynomials for accurate force fields*, Phys. Rev. B **108**, 094102 (2023).
- [47] R.D. Johnson III (Ed.), *NIST Computational Chemistry Comparisons and Benchmark Database*, NIST Standard Reference Database, Number, Release **18**, NIST, Gaithersburg, MD, 2016.
- [48] Q. Sun, J. Yang, G. K-L. Chan, *A general second order complete active space self-consistent-field solver for large-scale systems*, Chem. Phys. Lett. **683**, 291-299 (2017).
- [49] S.Lehtola, *Assessment of initial guesses for self-consistent field calculations, Superposition of atomic potentials: simple yet efficient*, J. Chem. Theory Comput. **15**, 1593-1604 (2019).
- [50] R. Hoffmann, *An Extended Hückel Theory. I. Hydrocarbons*, J. Chem. Phys. **39**, 1397-1412 (1963).
- [51] J. Knap, et al, *Extended Hückel and Slater's rule initial guess for real space grid-based density functional theory*, Comput. Theor. Chem. **1062**, 24-29 (2015).
- [52] S.Lehtola, *Fully numerical calculations on atoms with fractional occupations and range-separated exchange functionals*, Phys. Rev. A **101**, 012516 (2020).

- [53] V.H.A. Nguyen and A. Lunghi, *Predicting tensorial molecular properties with equivariant machine learning models*, Phys. Rev. B **105**, 165131 (2022).